Preparation of High Conductivity Hierarchical Porous Carbon Based on Sodium Lignosulfonate with Pre-crosslinking

Yanjie Yi, Yi Hou,* and Youming Li

The electrode material plays a key role in the performance of a supercapacitor. This study reports a method to prepare high conductivity hierarchical porous carbon with pre-crosslinking based on sodium lignosulfonate, which usually is burned as a waste effluent in pulp and paper mills. Results indicate pre-crosslinking with glutaraldehyde and ethyleneimine polymer, activation with less potassium hydroxide KOH, and finally carbonization to form carbon materials of hyperbranched macromolecules with ultra-rich specific surface area of 2780 m^2/g and reasonable pore size distribution. The prepared carbon material showed high specific capacitance and good electrochemical performance when used as electrode materials for supercapacitors. At 0.5 A/g, the specific capacitance was 305 F/g, and the specific capacitance decay was only 6.2%, even after 2500 consecutive charge/discharge cycles, which revealed the huge potential for the supercapacitor characteristics with long service life. The results provided a high-valued application of industrial waste, which is important to further the sustainable development of the national economy.

Keywords: Sodium lignosulfonate; Porous carbon; Supercapacitor; Pre-crosslinking

*Contact information: State Key Laboratory of Pulp and Paper Engineering, South China University of Technology, 510640, Guangzhou, China; *Corresponding author: ceyhou@scut.edu.cn*

INTRODUCTION

With the development of society and technology and the increased demand for energy, the high-performance capacitor has attracted a lot of attention. The supercapacitor has the characteristics of high charging and discharging speed, high efficiency, environmental friendliness, long cycle life, wide application temperature range and high safety performance, and ease of use as a fast charging and discharging standby power (Mao *et al.* 2017; Gao *et al.* 2018; Men *et al.* 2019; Sun *et al.* 2019). The electrode of the supercapacitor is composed of carbon materials with high specific surface area (Beguin *et al.* 2014). Recently, biomass-based porous carbon materials have been attracting extensive attention as a way to achieve high utilization of resources. Various biomass resources, such as bamboo (Zhang *et al.* 2018), rice husk (Kumagai *et al.* 2013), corn stover (Kumagai *et al.* 2013), and tea (Song *et al.* 2019), have been used in the preparation of porous carbon to be then applied in supercapacitors.

At present, the preparation method of biomass porous carbon is mainly concentrated as a chemical activation method; the activator is mostly potassium hydroxide (KOH), and the carbon-alkali ratio is 1:3. High alkali consumption not only increases the production cost but also corrodes the carbonized instrument and reduces its service life. The prepared porous carbons are greatly influenced by the structure of the precursors. Different precursor structures lead to different pore structures of porous carbon. The

random staggered arrangement between the pore channels results in lower electrolyte ion transport efficiency, high resistance, and lower capacitance utilization. Doping heteroatoms to the carbon framework can improve the wetting performance of the surface (Wang *et al*. 2020), storing a large number of ions. The presence of heteroatoms can form the center of redox reaction and thus introduce Faraday pseudocapacitors. For example, Wang *et al*. (2019) and Liu *et al*. (2019) prepared O-N-S co-doped hierarchical porous carbons to improve the specific capacitance.

As a by-product of pulping and papermaking, lignin and its derivatives are mostly excreted in the form of black liquid (Lora and Glasser 2002). Black liquor is usually burned, such that lignin and other organic compounds are not effectively used. This is a great waste of resources. As natural aromatic compounds, the carbon content of the lignin is as high as 60 to 70%; in addition, lignin is one of the most abundant organic matters in the natural world (Aro and Fatehi 2017). In recent years, Chang *et al.* (2016) attempted to prepare lignin directly into porous carbon using chemical activations. However, the prepared porous carbons have the disadvantages of relatively small specific surface areas, unreasonable pore size distribution on the carbon skeleton, difficulties to control the pore formation process during the carbonization process, and the poor electrochemical performance after assembling into capacitors. Later, Zhang *et al.* (2019) proposed a novel green bacterial activation method for the synthesis of lignin-based porous carbon materials. Under the treatment of bacterial decomposition, the specific surface area of the carbon precursor is improved, which has a positive effect on the subsequent carbonization process, but colony growth requires high environmental and material requirements, and the internal treatment of carbon precursor is not uniform, resulting in a large difference of carbon structure. Therefore, a simple and easy pretreatment method of precursors is necessary for the preparation of porous carbon with high specific area and high electrochemical performance.

In this work, porous carbon materials were prepared by the innovative introduction of pre-crosslinking reaction using lignin sulfonate produced in the pulping and papermaking process as the raw material. To explore the influence of pre-crosslinking and activation processes on the pore size, surface area, and electrochemical properties of carbon materials, it can provide a new technical route and data base for the high-value application of biomass resources.

EXPERIMENTAL

Materials

Sodium lignosulfonate (93 wt%) was obtained from Damas-Beta Corporation (Guangzhou, China). It was used without any further purification. Glutaraldehyde solution (25%) was purchased from Kermel Reagent Co., Ltd. (Tianjing, China). Ethleneimine polymer (M.W. 1800.99%) was purchased from Innochem Company (Beijng, China). Potassium hydroxide (KOH), hydrochloric acid (HCl), and ethanol absolute were all of analytical grade and purchased from Guangzhou Congyuan Fine Chemical Co., Ltd. (Guangzhou, China). Deionized water was used in all experiments.

Synthesis

Preparation of carbon materials

A total of 5 g sodium lignosulfonate was dissolved in 60 mL ethanol absolute, 2.5 g glutaraldehyde aqueous solution was added, 0.01 mol ethyleneiminepolymer was added as a crosslinking agent, the mixed solution was stirred, and ultrasonic treatment was applied for 1 h. The mixed solution was transferred into the polytetrafluoroethylene and reacted for 8 h at 160 °C. After the reaction was finished, the mixed solution was cooled to room temperature, washed with ethanol absolute, and dried at 60 °C. Precursor after pre-crosslinking reaction (labeled as SLP) was heated to 400 °C at the rate of 2 °C/min and pre-carbonized for 1 h at 400 °C. The pre-carbonation sample was mixed with KOH (1:1) and carbonized at 800 °C for 2 h at the rate of 4 °C/min. The porous carbon material hereafter referred to as SLPA (sodium lignosulfonate that had undergone pre-crosslinking and activating) was obtained after being washed with 1 mol/L HCl and deionized water to pH = 7.

For comparison, the sample called SLPC (sodium lignosulfonate that had undergone pre-crosslinking but without activating) was synthesized by following the same process without KOH as activator. Sodium lignosulfonate directly carbonized without pre-crosslinking or activator was named SLC. Sodium lignosulfonate using KOH as activators but without pre-crosslinking reaction were marked as SLAC.

Methods

Characterization

The 3D morphology and microstructures of carbon powders were observed by a LEO1530VP scanning electron microscope (SEM) (Carl Zeiss Co., Ltd., ShangHai, China). The specific surface and density functional theory were studied with the Brunauer-Emmett-Teller (BET) method using N_2 adsorption-desorption at 77 K after treating the samples at 300 °C for 8 h. X-ray photoelectron spectroscopy (XPS) (Thermol/ESCALAB 250XI; (Thermo Fisher Scientific Co., Ltd., Waltham, America) was conducted to examine the surface chemical compositions of the samples. The crystallographic information of the samples was investigated using a Bruker D8 Advanced X-ray diffractometer (XRD) with Cu Kα1 radiation source and Raman spectroscopy (LabRAM Aramis, Paris, France).

Electrochemical characterization

The performances of the samples were first evaluated using a three-electrode system in an electrochemical workstation (CHI660E; CH Instruments Co., Ltd., Shanghai, China). In a three-electrode system, the SLPA electrode, platinum electrode, and Ag/AgCl electrode were used as the working electrode, counter electrode, and reference electrode, respectively. To prepare working electrodes, the samples, acetylene black, and polytetrafluoroethylene (PTFE) were mixed in a weight ratio of 8:1:1, followed by addition of absolute ethanol to make the mixture into a uniform slurry. After drying at 120 °C for 8 h, the mixture was pressed onto nickel foam as the current collector.

The electrochemical characterization, such as cyclic voltammetry (CV), galvanostatic charging-discharging (GCD), and electrochemical impedance spectroscopy (EIS), measurements were conducted using 6 M KOH in the voltage range of -1 to 0 V.

The specific capacitance of electrode was calculated using Eq. 1,

$$C_m = I \times \Delta t / (m \times \Delta V) \quad (1)$$

where C_m (F g^{-1}) is specific capacitance, Δt (s) is discharge time, m (g) is active material mass, and ΔV (V) is the potential window.

RESULTS AND DISCUSSIONS

Fabrication of SLPA Carbon Composites

The synthesis mechanism of SLPA is depicted in Schemes 1 and 2.

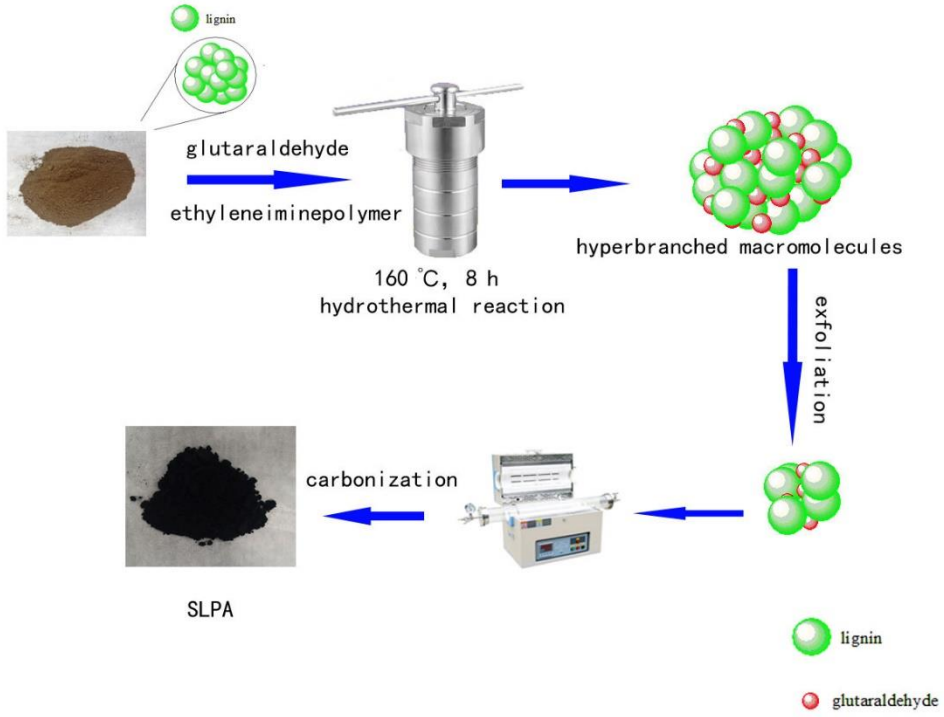

Scheme 1. Preparation process of the porous carbon

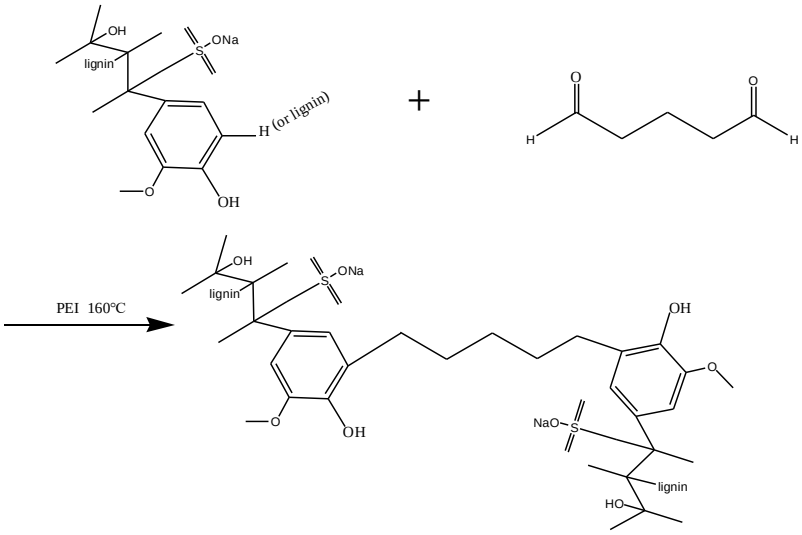

Scheme 2. Schematic diagram of the precursor preparation process

Due to the self-pressurization due to volatilization of the solvent in the hydrothermal reactor, the macromolecules undergo the processes of dissolution and crystallization (Barbier *et al.* 2012), resulting in the branched chain connected to the benzene ring breaking off, molecular complexity, and volume reduction. Hydroxyl groups on the benzene ring of sodium lignosulfonate and glutaraldehyde can react with the ethyleneimine polymer as a crosslinking agent. Due to the fracture of the branched chain, the linked molecules between the tightly connected sodium lignosulfonate macromolecules became smaller, and the whole surface of macromolecules became loose, so it is easy to form many and regular pores in the carbonation process. In the process of carbonization, due to the micropores present in the molecule, a more developed pore structure can be formed using less KOH as activator. The KOH etches the carbon skeleton to generate micro-pores, and the gas generated in the high-temperature carbonization process escapes to further amplify the pores to obtain carbon materials with ultra-high specific surface areas.

Materials Characterization

The SEM analysis can directly explore the morphology of the as-prepared samples. Figure 1 shows the 3D interconnected porous architecture.

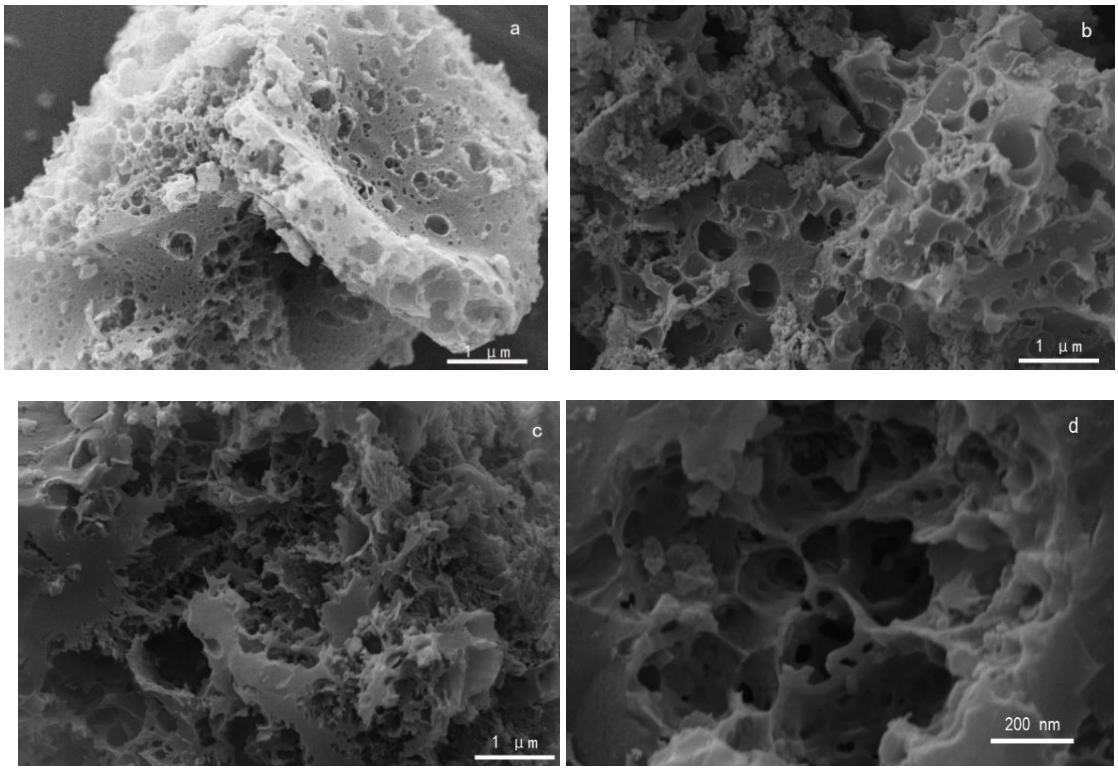

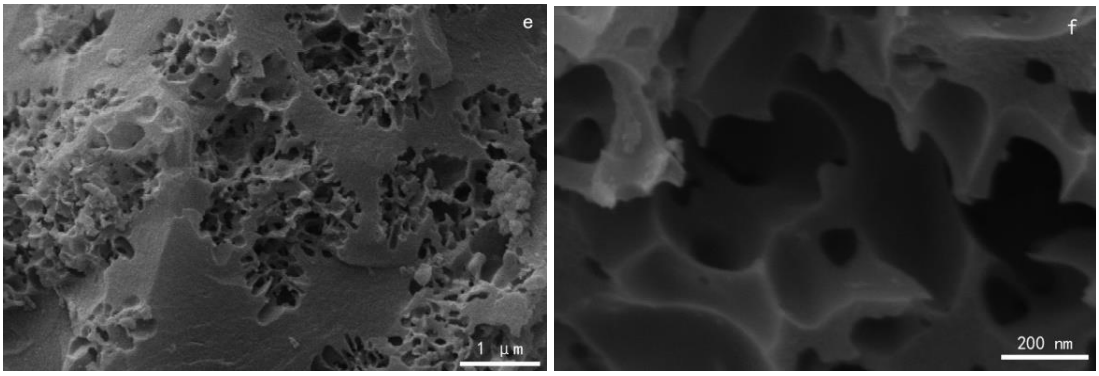

Fig. 1. SEM images of (a) SLC, (b) SLAC, (c and d) SLPC, and (e and f) SLPA

As shown in Fig. 1a, the SLC samples exhibited a loose and irregular porous structure. Most of the pores were mesopores, and the depth of the pores was shallow. The results showed that the samples without pre-crosslinking had the characteristics of small and underdeveloped pore size in the carbonization process. Figure 1b demonstrates that the pores of SLAC samples became expanded, deeper, and the carbon bone was hard, indicating that the activators increased the number of pores and expanded pore size during the carbonization process. From Figs. 1c and 1d, the holes were interlaced and further deepened, and a large number of micropores appeared on the inner wall of the macrospores. At the same time, the surface of carbon material has the tendency of gradually becoming smooth. This phenomenon indicated that the pre-crosslinking reaction can increase the number of pore-forming active sites in the carbonization process, and it was easy to form a large number of micropores. With the carbonization process, the pores sizes were enlarged, the pore walls were thickened, and the internal stability of carbon structures were improved. Figures 1e and 1f show the morphology of the SLPA samples. The graphitization of SLPA increased and the pores became deeper and the pore sizes further increased compared to the SLPC. The pores contained a large number of micropores, and the wall was thickened. It was easy to find that the surface of the prepared carbon materials contained a large number of well-developed pores and the surface of carbon materials also became more smooth and the size of the pores were uniformed under the synergistic action of the pre-crosslinking reaction and activators.

The structural characteristics of the samples were investigated by XRD. Two broad diffraction peaks were observed at 2θ = 23° and 43°, corresponding to the (002) and (101) graphitic carbon, respectively. The peaks that are evident in Fig. 2 implied that the samples had amorphous structure. Peaks of SLC were weaker and broader than others, showing a lower degree of graphitization.

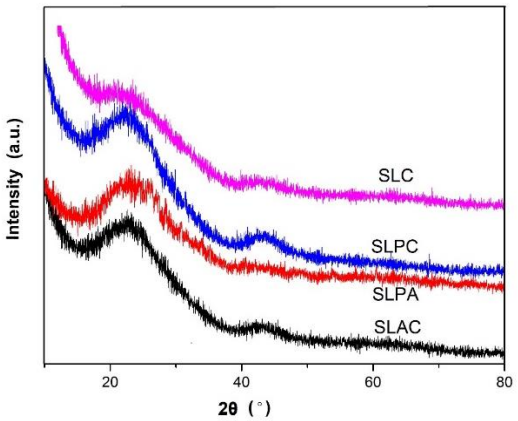

Fig. 2. The XRD patterns of SLC, SLAC, SLPC, and SLPA

Compared to the SLC and SLAC samples, the SLPC and SLPA samples (002) peaks were narrow and strong, indicating the extent of graphitization was obviously higher than that of others. This result suggested that the pre-crosslinking reaction had a positive effect on improving the graphitization of carbon materials in the subsequent carbonization process. A narrow and strong peak of SLPA at around 2θ = 26° showed the sample exhibited a high graphitization degree. These results were consistent with SEM images.

As shown in Fig. 3, the Raman spectroscopy of the samples were applied to verify the structural defects of them. Two peaks at around 1345 cm^{-1} (D-band for the structural defects), and 1589 cm^{-1} (G-band for the structural defects) can be observed. The graphitization extent of the samples can be calculated from the intensity ratio (I_D/I_G). The I_D/I_G values for SLC, SLAC, SLPC, and SLPA were 1.050, 1.045, 0.999, and 0.949, respectively. Clearly, the SLPA had the lowest ratio, revealing its lowest degree of structural disorder and higher graphitization. The SLPC sample just had more of a pre-crosslinking process than the SLC, and the other conditions remained the same. However, from the I_D/I_G values, the graphitization degree of the SLPC was greatly improved, which indicated that the pre-crosslinking treatment can improve the order degree of precursors and had a positive effect on the carbonization process. The authors can also draw the same conclusion from the I_D/I_G values of the SLPA and SLAC. The increase of graphitization degree can make up the carbon defect and improve the conductivity (Barranco *et al.* 2010).

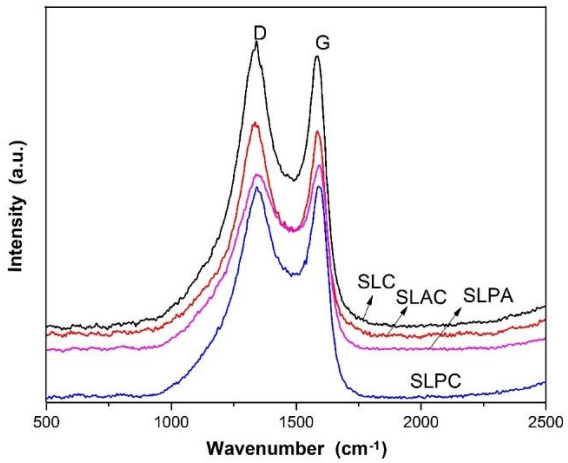

Fig. 3. Raman spectra of SLC, SLAC, SLPC, and SLPA

The XPS method was employed to investigate the elemental composition and chemical structure of the carbon samples. Table 1 lists the C and O contents of the four samples, respectively. Figure 4a shows that the XPS survey spectra contained two peaks of carbon, *i.e.* the (C1s peak) and (O1s peak). As shown in Figs. 4b through e, the peaks of C1s were found at 284.4, 285.6, 286.5, and 289.2 eV, and they were assigned to C=C/C-C, C-O, C=O, and O=C-O, respectively (Ai *et al.* 2015; Gharehkhani *et al.* 2015). Compared to the other three samples, the enhanced C-O peaks in the spectrum of the SLPA samples revealed that the sample SLPA had the highest oxygen content.

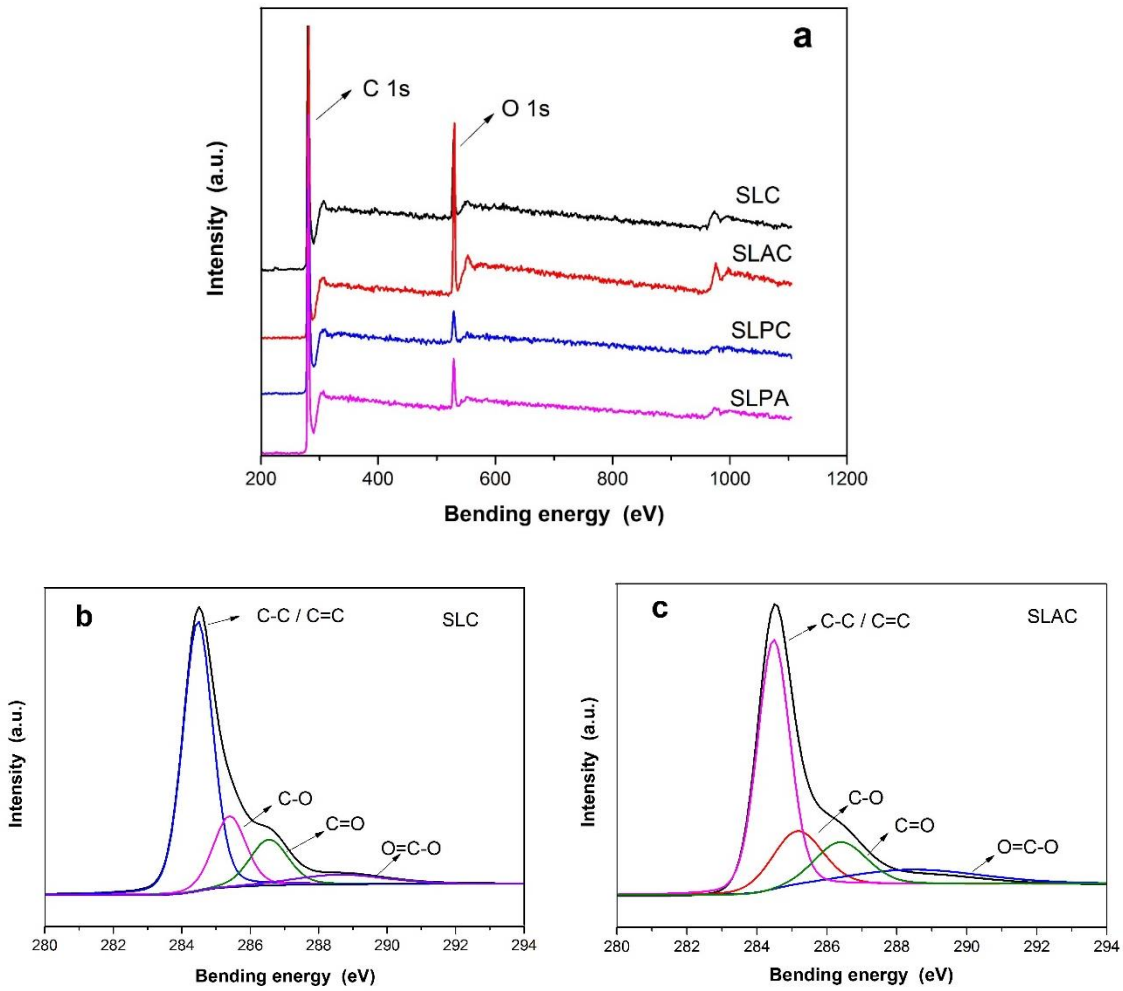

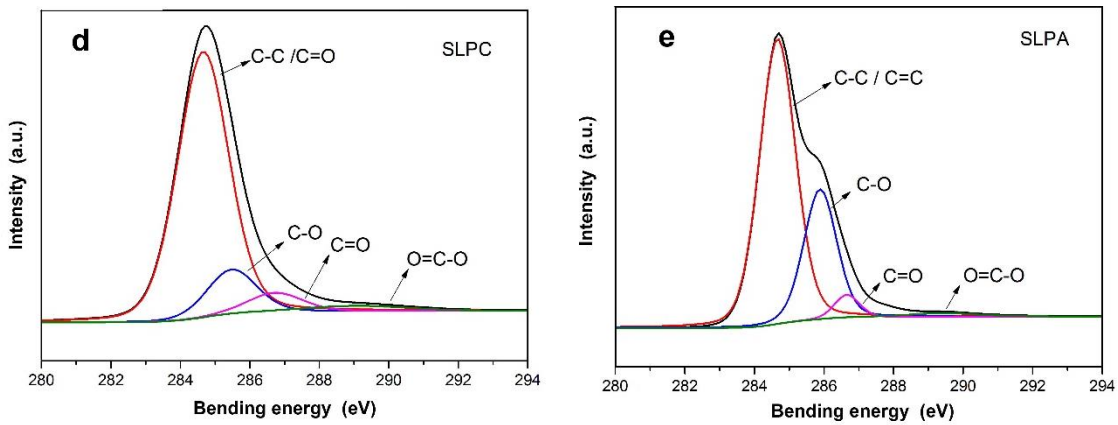

Fig. 4. Surface composition analysis of the samples: (a) XPS survey spectra of the samples; the high-resolution of C1s feature of (b) SLC; (c) SLAC; (d) SLPC; and (e) SLPA

Table 1. The Specific Surface Area and Pore Structure of the SLC, SLAC, SLPC, and SLPA

Content (%)	SLC	SLPC	SLAC	SLPA
C	83.21	84.51	87.60	87.54
O	8.42	7.99	9.68	9.76
others	8.37	7.50	2.72	2.70

Oxygen atoms doped on the carbon network could enhance the wettability and electrochemical activity and provide extra pseudocapacitance contribution (Wei *et al.* 2016). The incorporation of oxygen atoms on the surface of electrode materials will lead to redox reaction, thus introducing pseudocapacitance and increasing the specific capacitance of electrode materials. This inference coincides with the results of the electrochemical characterization.

The pore textures of the carbon samples were tested by nitrogen adsorption-desorption isotherms measurements. As shown in Fig. 5, four curves showed the typical IV-type isotherms according to the IUPAC classification (Thommes *et al.* 2015), in which an obvious intense increase in adsorption amount under low relative pressure can be found because of the existence of micropores. Under a medium relative pressure ($0.45 < p/p_0 < 0.9$), every sample showed a type H4 hysteresis loop that revealed carbon samples containing mesopores. At $p/p_0 > 0.9$, the curve slowly increased and demonstrated the presence of macropores.

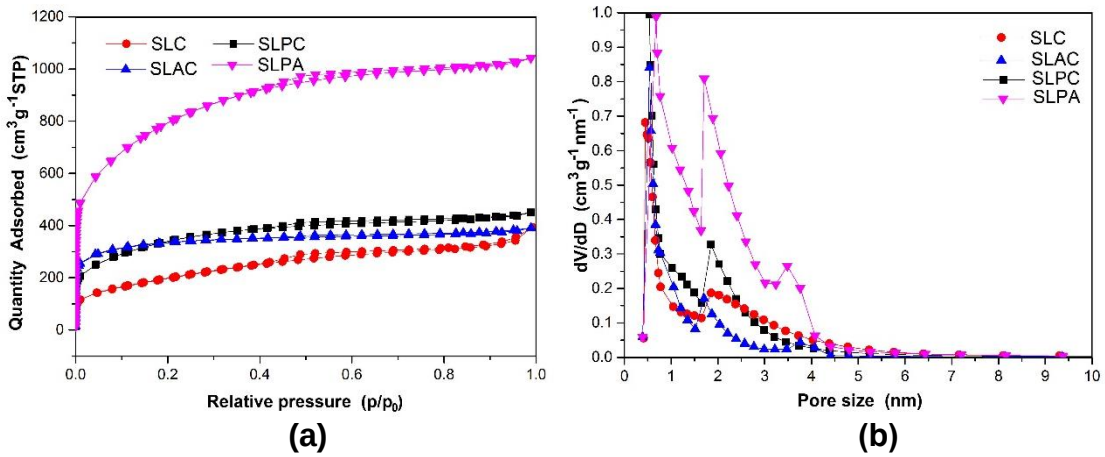

Fig. 5. (a) N_2 adsorption/desorption isotherms of the SLC, SLAC, SLPC, and SLPA; (b) Pore size distributions of the SLC, SLAC, SLPC, and SLPA

The porosity parameters of the as-prepared carbon samples are listed in Table 2. The SLPA samples had the highest specific surface area (2780 m^2/g) compared to SLC (716.5 m^2/g), SLAC (987.3 m^2/g), and SLPC (1190 m^2/g).

Table 3 compares the specific surface area of lignin-based porous carbon under different pretreatment methods. The authors found that the porous carbon prepared by the pre-linking reaction had the largest specific surface area. In the pre-crosslinking process, the outer layer of the macromolecule was far away from the nucleus. Consequently, it was less bound and was prone to fracture in the hydrothermal process. While many nucleations can be produced in the process, the broken chains around the nucleus formed new molecules with larger surface, smaller volume, and micropore framework, thus increasing the specific surface area of the precursors. Furthermore, from the pore size distribution, SLPA contained developed micropores and mesoporous pores. Those pores can provide a large number of storage space and transmission channels for electrons (Niu *et al.* 2017), which was in favor of the electrochemical performance of the samples.

Table 2. Specific Surface Area and Pore Structure of the SLC, SLAC, SLPC, and SLPA

Samples	S_{BET} (m^2/g)[a]	S_{mic} (m^2/g)[b]	S_{ext} (m^2/g)[c]	S_{mic}/S_{ext}	V_{total} (cm^3/g)[d]	D_m (nm)[e]
SLC	716.5	244.5	472.0	0.520	0.521	2.909
SLAC	987.3	583.4	403.9	1.450	0.584	2.367
SLPC	1188.3	220.4	967.9	0.228	0.673	2.265
SLPA	2782.0	639.2	2142.8	0.298	1.581	2.273

[a] S_{BET} is the total specific surface area;
[b] S_{mic} is the micropore specific surface area;
[c] S_{ext} is the external surface area ($S_{ext} = S_{BET} - S_{mic}$);
[d] V_{total} is the total pore volume;
[e] D_m is the average pore diameter.

Table 3. Comparison of the Specific Surface Area of the SLPA and Other Reported Lignin Based Porous Carbon

Precursor	Pretreatment Method	Area (m^2/g)	Ref.
Lignin	Bacteria decomposition	1831	a*
Lignin Oligomers	Thermal crosslinking	2120	b*
Alkali Lignin	AL/ZnC_2O_4 composite	365.3	c*
Enzymatic Hydrolysis Lignin	Microwave heating	2482	d*
Sodium Lignosulfonate	Pre-crosslinking	2782	This work

a* Zhang *et al.* (2019); b* Ho *et al.* (2018); c* Fu *et al.* (2019); d* Wang *et al.* (2019)

Electrochemical Evaluation

To evaluate the performance of the prepared carbon materials as electrode-active materials for supercapacitors, the capacitive performance of the samples were tested in a three-electrode system in 6 mol/L KOH electrolyte. As shown in Fig. 6a, at the scanning rate of 50 mV/s, all the CV curves had a rectangular shape, indicating a typical double-layer capacitive behavior. From Fig. 6a, two peaks are apparent at *ca.* -0.54 V and -0.32 V, which may be due to the redox reaction of oxygen atoms on the surface of the materials.The slight deviation from the ideal rectangular shape in the high potential can be observed in the CV curves of the SLPC and SLPA samples, which may be attributed to the presence of oxygen atoms that initiate the faradaic redox reactions and provide additional pseudocapacitance (Nian and Teng 2002; Chen *et al.* 2008; Ren *et al.* 2013). Furthermore, the surrounded area by the CV curve of SLPA was larger than that of SLC, SLAC, and SLPC, indicating the improvement of specific capacitance due to the dramatically increased surface area. The CV curves of the SLPA retained their quasi-rectangular shape as the scan rate increased from 10 mV/s to 200 mV/s (Fig. 6b), revealing good rate capability. In Figs. 6c and d, galvanostatic charge/discharge tests further evaluated the electrochemical performance of the samples. As shown in Fig. 6c, at the current density of 0.5 A/g, the calculated specific capacitance of the SLA, SLAC, SLPC, and SLPA samples was 75.7, 107, 245, and 305 F/g, respectively. The GCD curves of SLAC, SLPC, and SLPA samples had obvious platforms that appeared during the charging process, indicating the existence of pseudocapacitor behavior (Milczarek and Nowicki 2013; Suktha *et al.* 2015). Even at 0.5A/g low current density, the SLPA IR drop was not obvious, revealing that its conductivity was higher than other samples. The GCD curves of the sample SLPA at different current density presented in Fig. 6d displayed typical capacitor triangle shapes. Table 4 compares the electrochemical performance of lignin-based porous carbon under different preparation methods. From the comparison results, it can be found that the porous carbon had a high specific capacitance after pre-crosslinking treatment, indicating that the pre-crosslinking treatment had a positive effect on the electrochemical performance of porous carbon.

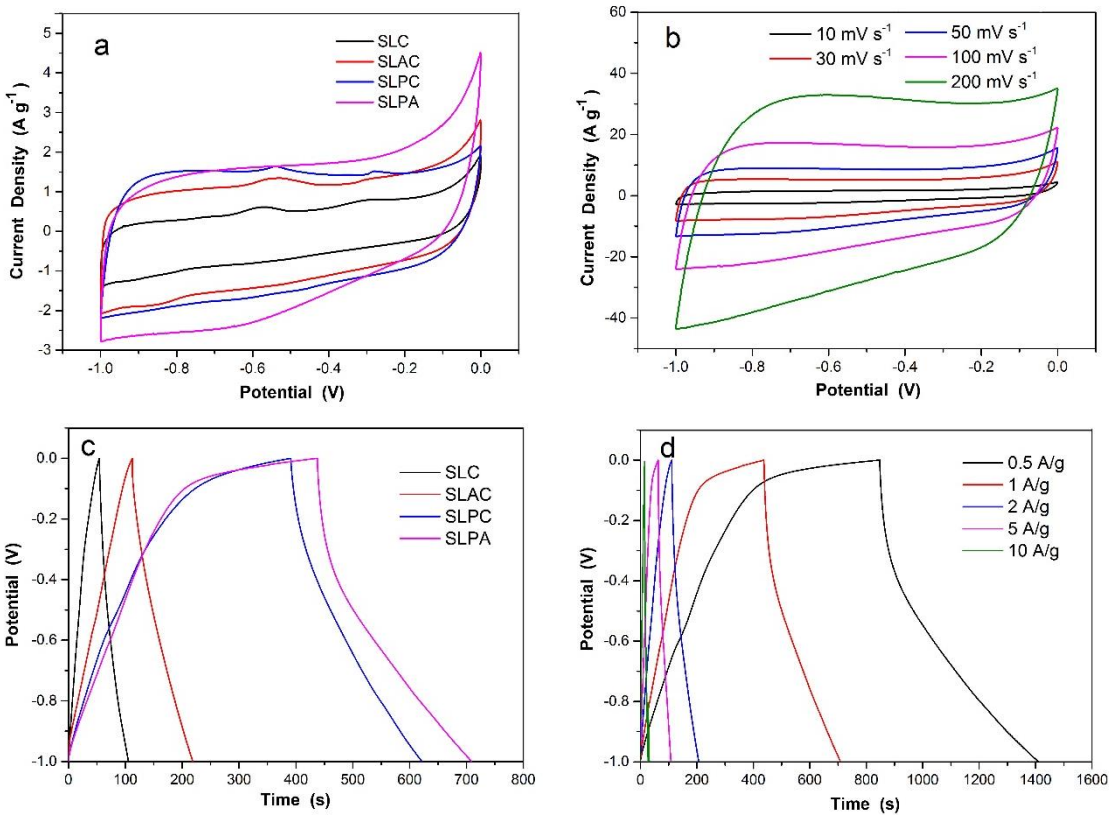

Fig. 6. Electrochemical performances of the prepared samples: (a) CV curves of the SLC, SLAC, SLPC, and SLPA samples at a scan rate of 50 mV/s; (b) CV curves of the SLPA at different scan rates; (c) GCD curves of the four samples at 1 A/g; (d) GCD curves of the SLPA at different current densities

Table 4. Comparison of Electrochemical Performance of Lignin-based Porous Carbon inder Different Preparation Methods

Precursors	Pretreatment Method	Test Conditions	Capacitance	Ref.
Lignin Oligomers	Thermal crosslinking	0.5 A/g	215 F/g	a**
Alkali Lignin	AL/ZnC_2O_4 composite	0.5 A/g	193 F/g	b**
Lignin	KOH as activator	0.5 A/g	269 F/g	c**
Lignosulphonate	SiO_2 as template	0.25 A/g	286 F/g	d**
Calcium Lignosulfonate	Without pretreatment	1 mA/cm^2	182 F/g	e**
Eucalyptus Kraft Lignin	CO_2 as activator	0.1 A/g	115 F/g	f**
Sodium Lignosulfonate	Pre-crosslinking	0.5 A/g	305 F/g	This work

a** Milczarek *et al.* (2013); b** Suktha *et al.* (2015); c** Tian *et al.* (2019); d** Zhao *et al.* (2015); e** Chen and Zhou (2012); f** Schlee *et al.* (2019)

On the basis of the GCD curves, the gravimetric capacitance of samples at different current densities are described in Fig. 7a. Due to the electrolyte ions diffusion capacity, the capacitance response was limited with the current density increases, resulting in a lower gravimetric capacitance. The SLPA still maintained a high gravimetric capacitance of 227 F/g at 5 A/g, which means a good rate capability. The Nyquist plots and equivalent circuit (Nian and Teng 2002; Graca *et al.* 2012; Ren *et al.* 2013) of the four samples are shown in Fig. 7b. In the low frequency range the Nyquist plot curves of the SLAC, SLPC, and SLPA

samples tended to be perpendicular to the real axis, showing typical features of EDL. However, that part of the SLC sample was far from the vertical axis, indicating that the capacitance utilization rate of the electrode material was low (Tian *et al.* 2015). In the high-frequency region, the Nyquist plot curves all tended to be semicircular. The diameter of the semicircle represents the charge transfer resistance between the electrode and the electrolyte (R_s) (Yuan *et al.* 2013). The intercept of the semicircle on the real axis represents the resistance of the ion transfer to the active material (R_{ct}) (Yuan *et al.* 2013). Variable R_s and R_{ct} were calculated and displayed in Table 5. The SLAC, SLPC, and SLPA samples all had low R_s and R_{ct}, indicating that they had excellent electrical conductivity, developed porous structure, and high mesoporous content. Due to the pore structures being underdeveloped and the mesopores being less, the R_{ct} of SLC was larger than other samples, resulting in a larger transport resistance of electrolyte ions.

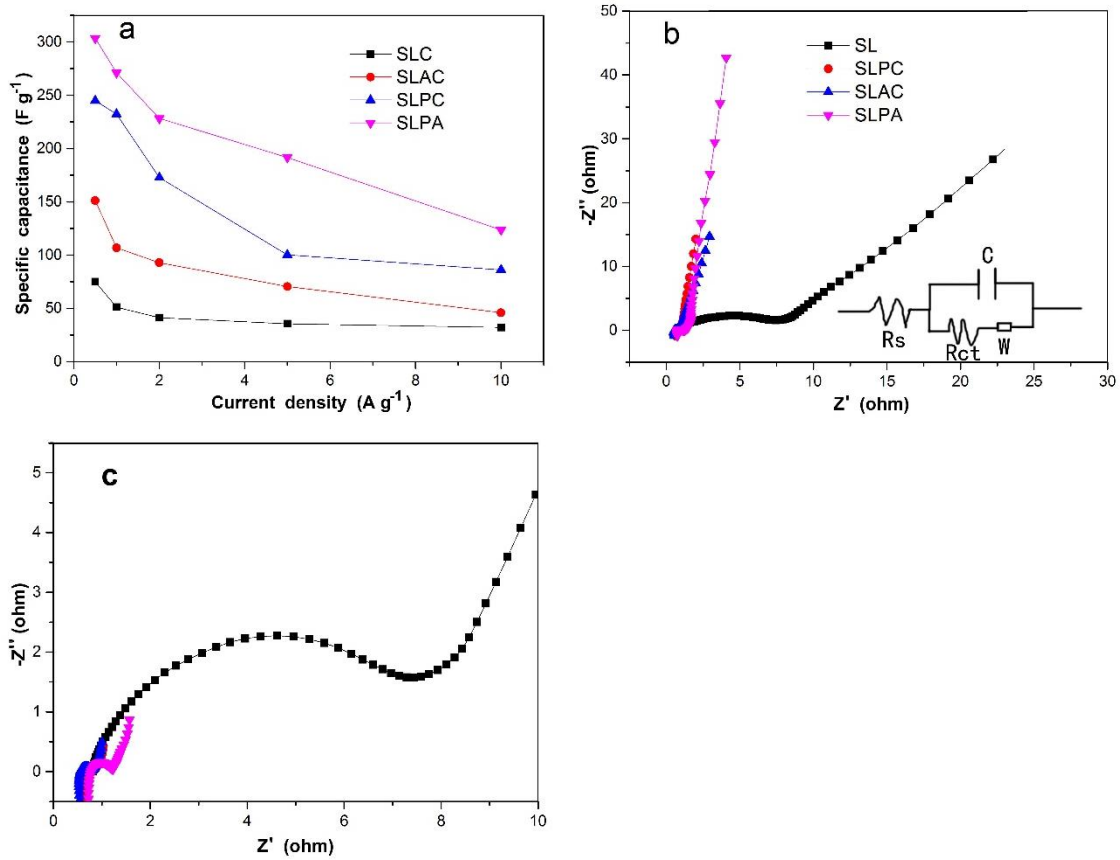

Fig. 7. (a) Specific capacitance curves of the SLC, SLAC, SLPC, and SLPA samples at different current densities; (b) Nyquist plots of the four samples; (c) Magnification in the high-frequency region and equivalent circuit diagram

Table 5. Resistance Values of the Prepared Samples

Element	SLC	SLAC	SLPC	SLPA
R_s (Ω)	0.81	0.64	0.56	0.78
R_{ct} (Ω)	6.46	0.14	0.25	0.44

The electrochemical stability of the SLPA was evaluated using continuous galvanostatic charge/discharge test at a current density of 10 A/g. The results in Fig. 7c show that the material had good charge/discharge stability, the capacitance retention was 93.8% after 2500 cycles.

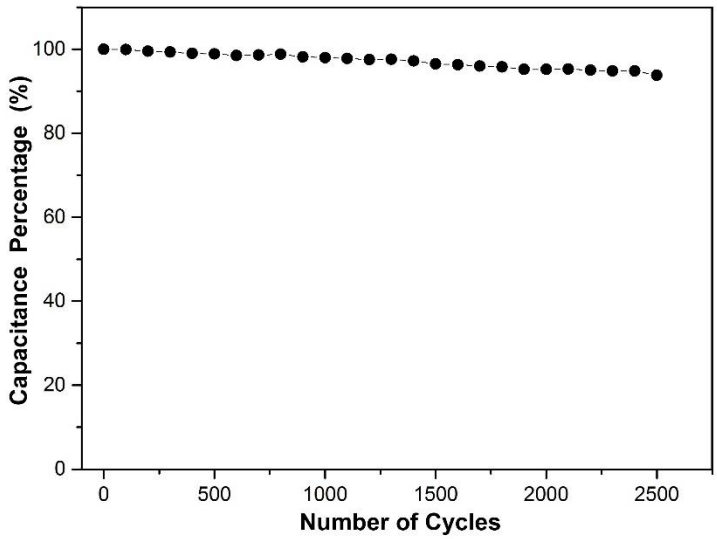

Fig. 8. Cycling stability of the SLC, SLAC, SLPC, and SLPA samples at a constant current of 10 A/g

CONCLUSIONS

1. The pre-crosslinking process had a positive effect on the formation of porous carbon. The formation of precursors with a large number of micropores can significantly reduce the amount of subsequent activators, optimize the pore size distribution, and improve the specific surface area (2780 m^2/g). The prepared porous carbon materials used in supercapacitors can significantly improve the performance of capacitors.
2. In a three-electrode system, the porous carbon material exhibited a high specific capacitance of 305 F/g at 0.5 A/g. Under high current density of 10 A/g, the capacitance can retain 93.8% of its initial value after 2500 consecutive charge/ discharge cycles.

REFERENCES CITED

Aro, T., and Fatehi, P. (2017). "Production and application of lignosulfonates and sulfonated lignin," *ChemSusChem* 10(9), 861-1877. DOI: 10.1002/cssc. 2017 0082

Ai, L., Liu, X., and Jiang, J. (2015). "Synthesis of loofah sponge carbon supported bimetallic silver-cobalt nanoparticles with enhanced catalytic activity towards hydrogen generation from sodium borohydride hydrolysis," *Journal of Alloys and Compounds* 625, 164-170. DOI: 10.1016/j.jallcom.2014.11.135

Barbier, J., Charon, N., Dupassieux, N., Loppinet-Serani, A., Mahé, L., Ponthus, J., Courtiade, M., Ducrozet, A., Quoineaud, A., and Cansell, F. (2012). "Hydrothermal conversion of lignin compounds. A detailed study of fragmentation and condensation reaction pathways," *Biomass and Bioenergy* 46(SI), 479-491. DOI: 10.1016/j.biombioe.2012.07.011

Barranco, V., Lillo-Rodenas, M. A., Linares-Solano, A., Oya, A., Pico, F., Ibañez, J., Agullo-Rueda, F., Amarilla, J. M., and Rojo. J. M. (2010). "Amorphous carbon nanofibers and their activated carbon nanofibers as supercapacitor electrodes," *Journal of Physical Chemistry C* 114(22), 10302-10307. DOI: 10.1021/jp1021278

Beguin, F., Presser, V., Balducci, A., and Frackowiak, E. (2014). "Carbons and electrolytes for advanced supercapacitors," *Advanced Materials* 26(14), 2219-2251. DOI: 10.1002/adma.201304137

Chang, Z., Yu, B., and Wang, C. (2016). "Lignin-derived hierarchical porous carbon for high-performance supercapacitors," *Journal of Solid State Electrochemistry* 20(5), 1405-1412. DOI: 10.1007/s10008-016-3146-2

Chen, X. Y., and Zhou, Q. Q. (2012). "The production of porous carbon from calcium lignosulfonate without activation process and the capacitive performance," *Lectrochimica Acta* 71, 92-99. DOI: 10.1016/j.electacta.2012.03.166

Chen, X. L., Li, W. S., Tan, C. L., Li, W., and Wu, Y. Z. (2008). "Improvement in electrochemical capacitance of carbon materials by nitric acid treatment," *Journal of Power Sources* 184(2), 668-674. DOI: 10.1016/j.jpowsour.2008.05.073

Fu, F. B., Yang, D. J., Wang, H., Qian, Y., Yuan, F., Zhong, J. Q., and Qiu, X. Q. (2019). "Three-dimensional porous framework lignin-derived carbon/ZnO composite fabricated by a facile electrostatic self-assembly showing good stability for high-performance supercapacitors," *ACS Sustainable Chemistry and Engineering* 7(19), 16419-16427. DOI: 10.1021/acssuschemeng.9b03521

Gao, Z. Y., Chen, C., Chang, J. L., Chen, L. M., Wang, P. Y., Wu, D. P., Xu, F., and Jiang, K. (2018). "Porous Co_3S_4@Ni_3S_4 heterostructure arrays electrode with vertical electrons and ions channels for efficient hybrid supercapacitor," *Chemical Engineering Journal* 343, 572-582. DOI: 10.1016/j.cej.2018.03.042

Gharehkhani, S., Shirazi, S. F. S., Jahromi, S.P., Sookhakian, M., Baradaran, S., Yarmand, H., Oshkour, A. A., Kazi, S. N., and Basirun, W. J. (2015). "Spongy nitrogen-doped activated carbonaceous hybrid derived from biomass material/graphene oxide for supercapacitor electrodes," *RSC Advances* 5(51), 40505-40513. DOI: 10.1039/c5ra01525a

Graca, M. P. F., Rudnitskaya, A., Faria, F. A. C., Evtuguin, D. V., Gomes, M. T. S. R., Oliveira, J. A. B. P., and Costa, L. C. (2012). "Electrochemical impedance study of the lignin-derived conducting polymer," *Electrochimica Acta* 76, 69-76. DOI: 10.1016/j.electacta.2012.04.155

Ho, H. C., Nguyen, N. A., Meek, K. M., Alonso, D. M., Hakim, S. H., and Naskar, A. K. (2018). "A solvent-free synthesis of lignin-derived renewable carbon with tunable porosity for supercapacitor electrodes," *ChemSusChem* 11(17), 2953-2959. DOI: 10.1002/cssc.201800929

Kumagai, S., Sato, M., and Tashima, D. (2013). "Electrical double-layer capacitance of micro- and mesoporous activated carbon prepared from rice husk and beet sugar," *Electrochimica Acta* 114, 617-626. DOI: 10.1016/j.electacta.2013.10.060

Lora, J. H. and Glasser, W. G. (2002). "Recent industrial applications of lignin: A sustainable alternative to nonrenewable materials," *Journal of Polymers and the Environment* 10(1-2), 39-48. DOI: 10.1023/A:1021070006895

Liu, F., Wang, Z. X., Zhang, H. T., Jin, L., Chu, X., Gu, B. N., Huang, H. C., and Yang, W. Q. (2019). "Nitrogen, oxygen and sulfur co-doped hierarchical porous carbons toward high-performance supercapacitors by direct pyrolysis of kraft lignin," *Carbon* 149, 105-116. DOI: 10.1016/j.carbon.2019.04.023

Men, B., Guo, P. K., Sun, Y. Z., Tang, Y., Chen, Y. M., Pan, J. Q., and Wan, P. Y. (2019). "High-performance nitrogen-doped hierarchical porous carbon derived from cauliflower for advanced supercapacitors," *Journal of Materials Science* 54(3), 2446-2457. DOI: 10.1007/s10853-018-2979-8

Milczarek, G., and Nowicki, M. (2013). "Carbon nanotubes/kraft lignin composite: Characterization and charge storage properties," *Materials Research Bulletin* 48(10), 4032-4038. DOI: 10.1016/j.materresbull.2013.06.022

Mao, N., Wang, H. L., Sui, Y., Cui, Y. P., Pokrzywinski, J., Shi, J., Liu, W., Chen, S. G., Wang, X., and Mitlin, D. (2017). "Extremely high-rate aqueous supercapacitor fabricated using doped carbon nanoflakes with large surface area and mesopores at near-commercial mass loading," *Nano Research* 10(5), 1767-1783. DOI: 10.1007/s12274-017-1486-6

Nian, Y. R. and Teng, T. S. (2002). "Nitric acid modification of activated carbon electrodes for improvement of electrochemical capacitance," *Journal of the Electrochemical Society* 149(8), A1008-A1014. DOI: 10.1149/1.1490535

Niu, Q., Gao, K. Z., Tang, Q. H., Wang, L. Z., Han, L. F., Fang, H., Zhang, Y., Wang, S. W., and Wang, L. X. (2017). "Large-size graphene-like porous carbon nanosheets with controllable N-doped surface derived from sugarcane bagasse pith/chitosan for high performance supercapacitors," *Carbon* 123, 290-298. DOI: 10.1016/j.carbon.2017.07.078

Ren, T. Z., Liu, L., Zhang, Y. Y., and Yuan, Z. Y. (2013). "Nitric acid oxidation of ordered mesoporous carbons for use in electrochemical supercapacitors," *Journal of Solid State Electrochemistry* 17(8), 2223-2233. DOI: 10.1007/s10008-013-2088-1

Schlee, P., Hosseinaei, O., Baker, D., Landmer, A., Tomani, P., Jose Mostazo-Lopez, M., Cazorla-Amoros, D., Herou, S., and Titirici, M. M. (2019). "From waste to wealth: From kraft lignin to free-standing supercapacitors," *Carbon* 145, 470-480. DOI: 10.1016/j.carbon.2019.01.035

Song, X. Y., Ma, X. L., Li, Y., Ding, L., and Jiang, R. Y. (2019). "Tea waste derived microporous active carbon with enhanced double-layer supercapacitor behaviors," *Applied Surface Science* 487, 189-197. DOI: 10.1016/j.apsusc.2019.04.277

Suktha, P., Chiochan, P., Iamprasertkun, P., Wutthiprom, J., Phattharasupakun, N., Suksomboon, M., Kaewsongpol, T., Sirisinudomkit, P., Pettong, T., and Sawangphruk, M. (2015). "High-performance supercapacitor of functionalized carbon fiber paper with high surface ionic and bulk electronic conductivity: effect of organic

functional groups," *Electrochimica Acta* 176, 504-513. DOI: 10.1016/j.electacta.2015.07.044

Sun, Q., Li, Y., and He, T. (2019). "The excellent capacitive capability for N,P-doped carbon microsphere/reduced graphene oxide nanocomposites in H_2SO_4/KI redox electrolyte," *Journal of Materials Science* 54(10), 7665-7678. DOI: 10.1007/s10853-019-03414-x

Thommes, M., Kaneko, K., Neimark, A., Olivier, J. P., Rodriguez-Reinoso, F., Rouquerol, J., and Sing, K. S. W. (2015). "Physisorption of gases, with special reference to the evaluation of surface area and pore size distribution (IUPAC Technical Report)," *Pure and Applied Chemistry* 87(9-10), 1051-1069. DOI: 10.1515/pac-2014-1117

Tian, J. Y., Liu, C. Y., Lin, C., and Ma, M. Y. (2019). "Constructed nitrogen and sulfur codoped multilevel porous carbon from lignin for high-performance supercapacitors," *Journal of Alloys and Compounds* 789, 435-442. DOI: 10.1016/j.jallcom.2019.03.070

Tian, W. Q., Gao, Q. M., Tan, Y. L., Yang, K., Zhu, L. H., Yang, C. X., and Zhang, H. (2015). "Bio-inspired beehive-like hierarchical nanoporous carbon derived from bamboo-based industrial by-product as a high performance supercapacitor electrode material," *Journal of Materials Chemistry A* 3(10), 5656-5664. DOI: 10.1039/c4ta06620k

Wei, X. J., Jiang, X. Q., Wei, J. S., and Gao, S. Y. (2016). "Functional groups and pore size distribution do matter to hierarchically porous carbons as high-rate-performance supercapacitors," *Chemistry of Materials* 28(2), 445-458. DOI: 10.1021/acs.chemmater.5b02336

Wang, X., Liu, Y. C., Chen, M. Z., Luo, M., Yang, P., Chen, W. M., and Zhou, X. Y. (2019). "Direct microwave conversion from lignin to micro/meso/macroporous carbon for high-performance symmetric supercapacitors," *ChemElectroChem* 6(18), 4789-4800. DOI: 10.1002/celc.201901315

Wang, Y.H., Wang, M. H., Wang, Z. W., Wang, S. M., and Fu, J. W. (2020). "Tunable-quaternary (N, S, O, P)-doped porous carbon microspheres with ultramicropores for CO2 capture," *Applied Surface Science* 507, article no. 145130. DOI: 10.1016/j.apsusc.2019.145130

Wang, Z. W., Wang, K., Wang, Y.H., Wang, S. M., Chen, Z. M., Chen, J. F., and Fu, J. W. (2019). " Large-scale fabrication of N-doped porous carbon nanosheets for dye adsorption and supercapacitor applications," *Nanoscale* 11(18), 8785-8797. DOI: 10.1039/c9nr01777a

Yuan, L. Y., Yao, B., Hu, B., Huo, K. F., Chen, W., and Zhou, J. (2013). "Polypyrrole-coated paper for flexible solid-state energy storage," *Energy and Environmental Science* 6(2), 470-476. DOI: 10.1039/c2ee23977a

Zhang, K. J., Liu, M. G., Zhang, T. Z., Min, X. Y., Wang, Z. G., Chai, L. Y., and Shi, Y. (2019). "High-performance supercapacitor energy storage using a carbon material derived from lignin by bacterial activation before carbonization," *Journal of Materials Chemistry A* 7(47), 26838-26848. DOI: 10.1039/c9ta04369a

Zhang, G. X., Chen, Y. M., Chen, Y. G., and Guo, H. B. (2018). "Activated biomass carbon made from bamboo as electrode material for supercapacitors," *Materials Research Bulletin* 102, 391-398. DOI: 10.1016/j.materresbull.2018.03.006

Zhao, Z. H., Hao, S. M., Hao, P., Sang, Y. H., Manivannan, A., Wu, N. Q., Liu, H. (2015). "Lignosulphonate-cellulose derived porous activated carbon for supercapacitor electrode," *Journal of Materials Chemistry A* 3(29), 15049-15056. DOI: 10.1039/c5ta02770e

Article submitted: July 2, 2020; Peer review completed: September 19, 2020; Revised version received: September 27, 2020; Accepted: October 3, 2020; Published: October 15, 2020.
DOI: 10.15376/biores.15.4.8995-9012